CBNOTE 292
CB Technical Report
Measurement of the Radiative Decay of $\omega \rightarrow \eta\gamma$

M. Lakata [a,1]

[a] *University of California, LBL, Berkeley, CA 94720, USA*

Id: sum.texx,v 1.8 1996/11/22 05:05:50 lakata Exp

The branching ratio of $\omega \rightarrow \eta\gamma$ has been measured: $\mathrm{BR}(\omega \rightarrow \eta\gamma) = (6.2 \pm 0.7_{\mathrm{stat}} \pm 1.0_{\mathrm{sys}}) \times 10^{-4}$.

1 Introduction

The radiative decays of mesons are a useful source in testing various theories of low energy physics, i.e. the quark model and the vector dominance model. For example, in both models, decays from and to nonet central states (i.e. η, η', ω, ϕ) are dependent on the pseudoscalar and vector mixing angles. For a review of radiative meson decays see [1]. All of the relevant low mass radiative meson decays have been observed, yet measurements of

$$\omega \rightarrow \eta\gamma \tag{1}$$

have been by far the poorest. The all neutral sources of ω production in $p\overline{p}$ annihilations is given in table 1. In this paper, the branching ratio of the decay of reaction 1 was measured using ω mesons from the two-body reaction

$$p\overline{p} \rightarrow \eta\omega \tag{2}$$

measured with the Crystal Barrel spectrometer[2] (PS197) at CERN. This proton-antiproton annihilation channel was the choice for analysis because, as a source for ω's, it has one of the highest branching ratios, has low combinatorics and is all neutral. The Crystal Barrel is especially suited for high

[1] This work forms part of the PhD thesis of Mark Lakata

Channel	BR	Ref	Comment
$p\overline{p}\rightarrow\gamma\omega$	$(6.8 \pm 1.9) \times 10^{-5}$	[4]	Too small
$p\overline{p}\rightarrow\pi^0\omega$	$(5.73 \pm 0.47) \times 10^{-3}$	[8]	Large $\pi^0\pi^0\eta$ background
$p\overline{p}\rightarrow\eta\omega$	$(1.51 \pm 0.12) \times 10^{-2}$	[8]	*Desired channel*
$p\overline{p}\rightarrow\omega\omega$	$(3.32 \pm 0.34) \times 10^{-2}$	[8]	Extra ω decay lowers net BR
$p\overline{p}\rightarrow\eta'\omega$	$(7.8 \pm 0.8) \times 10^{-3}$	[8]	η' hard to tag
$d\overline{p}\rightarrow\omega$n	$(2.28 \pm 0.41) \times 10^{-5}$	[9]	Too small
$p\overline{p}\rightarrow\pi^0\pi^0\omega$	$(2.57 \pm 0.17) \times 10^{-2}$	[22]	Many combinatorics
$p\overline{p}\rightarrow\pi^0\eta\omega$	$(6.8 \pm 0.5) \times 10^{-3}$	[10]	Many combinatorics
$p\overline{p}\rightarrow\rho^0\eta$	$(5.7 \pm 1.5) \times 10^{-3}$	[12]*	ρ^0 background.
$p\overline{p}\rightarrow\rho^0\pi^0$	$(1.7 \pm 0.1) \times 10^{-2}$	[12]*	ρ^0 background.
$p\overline{p}\rightarrow\pi^+\pi^-\omega$	$(6.6 \pm 0.6) \times 10^{-2}$	[11]	Charged split-offs

Table 1
Branching ratios of channels containing ω's or ρ^0's. * Indicates averages of many measurements.

precision gamma measurements. The channel $\eta\omega$ was chosen over $\pi^0\omega$ for two reasons. First, the former channel contains no π^0's at all, π^0's being produced by the potential feed-through reaction $\omega\rightarrow\pi^0\gamma$. Second, the potential ρ^0 backgrounds are a relative factor 9 times less in $\eta\omega/\eta\rho^0$ than in $\pi^0\omega/\pi^0\rho^0$.

After some preliminary work, we decided not to use the charged channel $p\overline{p}\rightarrow\pi^+\pi^-\omega$ because of the large problem of split-offs associated with charged particles, even though the branching ratio is the highest. Suppressing the split-offs is possible but greatly reduces the signal efficiency. The size of the backgrounds was also comparable those encountered in this analysis.

The ratio of rates of $\omega\rightarrow\eta\gamma$ to $\omega\rightarrow\pi^0\gamma$ was measured, thus requiring analysis of both these final states (of minimal gamma multiplicity) (see figure 5).

$$p\overline{p} \rightarrow \eta\omega\rightarrow\eta(\pi^0\gamma)\rightarrow(\gamma\gamma)\,((\gamma\gamma)\gamma) \quad (3)$$
$$p\overline{p} \rightarrow \eta\omega\rightarrow\eta(\eta\gamma)\rightarrow(\gamma\gamma)\,((\gamma\gamma)\gamma) \quad (4)$$

In the analysis, the gammas were combined pairwise to search for η's and π^0's. Once the π^0's and η's were identified, they were combined with the remaining unpaired gamma to form ω candidates.

Software	CMZ Version
CBOFF	1.30/04
BCTRAK	2.04/01
LOCATER	2.01/05
GTRACK	1.36/01
CCDBCB	2.05/00
CBGEANT	5.05/00,01,03,06

Table 2
Software Versions used

CB Run	0-prong Events
Jun 90	1,416,682
Jul 90	4,487,476
Sep/Oct 90	1,537,951
Nov 90	4,904,927
May 91	1,564,884
Jun 91	1,455,911
Aug 91	1,472,493
Oct 93	1,955,476
Jun 94	1,242,967
Total	19,365,050

Table 3
0-prong events analyzed. The total count is correct, however the counts for each run period are approximate.

2 Treatment of Data

The versions of the software are given in table 2. The small changes in CBGEANT between various MC data sets do not affect the results significantly.

See table 3.

The data set consisted of 19,365,050 triggered events of antiproton annihilation at rest in liquid hydrogen. The trigger required no hits in the proportional wire chambers surrounding the target, thus greating enhancing all neutral decays of antiproton-proton, which occur naturally with a probability of (3.9 ± 0.3) %, as measured previously in our experiment [5]. This data set is equivalent

Production Pass	Threshold (MeV)	
	Cluster	Secondary Photon
• Signal Enhancement	20	20
◦ Background Suppression	4	10

to nearly 5.0×10^8 antiproton-proton annihilations.

Photons deposit their energy in typically several neighboring CsI crystals, most energy being deposited in one crystal. The photon reconstruction software first identifies contiguous clusters of crystals with a signal above threshold, 1 MeV in this case. The cluster is accepted if the total energy of the crystals within the cluster is above another defined value, called the cluster threshold. It is likely that a cluster is the result of more than one photon, in the case were the photons have nearly the same direction and the showers overlap. Thus within each cluster, local maxima are assumed to be due to separate photons. Thus multi-photon clusters are accepted if the individual maxima are greater than another defined value, the secondary photon threshold.

For reasons that will be explained below, the desired signal efficiency is maximal when the aforementioned thresholds are relatively high, while the background is minimal when the thresholds are relatively low. As a compromise, the data is processed twice with different thresholds as shown in table 2. In the first pass, the thresholds are set to be high to enhance the signal. In the second pass, the thresholds are set to be low in order to positively identify background events and reject them. However, the reconstructed values from the second pass are discarded once the identified background events are rejected. The values given in the table for the signal enhancement pass were chosen at the point were the marginal increase of signal became smaller than the marginal increase in background. The values given for the background suppression pass are the lowest usable values that avoid the huge background due to very low energy split-offs (0-4 MeV).

Some slight scaling corrections were applied to the data and MC data sets, to bring the measured π^0, η and ω peak means as close to the PDG values as possible. The gamma energies of the data were scaled by 1.003 and the those of the MC were scaled by 0.998. To check these scalings, a Gaussian plus constant was fitted to the π^0 and η peaks in the $\gamma\gamma$ invariant mass plot, and to the ω peak in the $\pi^0\gamma$ invariant mass plot. The resulting mean values deviated from the PDG values by the following amounts:

peak	Fit Range	Δ MeV. in Data	Δ MeV. in MC
π^0	[120,150]	0.5 ± 0.1 %	0.5 ± 0.1 %
η	[525,575]	0.04 ± 0.1 %	-0.03 ± 0.1 %
ω	[750,810]	0.02 ± 0.1 %	-0.15 ± 0.1 %

Except for the π^0 mass, the scaling corrections produced adequate values. Note that it was impossible to have all three masses exactly correct, apparently due to non-linear errors in the original energies. However, the deviations were small enough to not affect the identification of π^0's and η's. For the fits described later, the MC was additionally scaled by 1.0025 (essentially cancelling the initial scaling of 0.998) to bring the centers of the ω peaks in MC and data as close together as possible. The additional systematic errors caused by this were probably negligible and ignored.

On this set of data, several initial cuts were made, shown in table 4. The signal enhancement parameters for the gamma reconstruction (see table 2), were used on the first pass through the data.

The first cut (1) required no reconstructed charged tracks. The second cut (2) made a loose cut on the total energy and momentum:

$$\vec{P}_i < 200 \text{ MeV}/c, \ (i = 1, 2, 3)$$

$$|E - 1876 \text{ MeV}/c^2| < 200 \text{ MeV}/c^2$$

The third cut (3) selected events with exactly five gammas. Finally, a χ^2 value was calculated for the event 4-momentum conservation hypothesis $p = (2m_p, 0, 0, 0)$, and a 10% confidence level cut was made in the fourth cut (4). These initial cuts eliminate 97% of the original data. The quality of the data can be seen in figure 1.

For cut five (5), a second pass was made through the data, but this time using the background suppression parameters for the gamma reconstruction (see table 2). The previous reconstructed gammas were set aside, and a new reconstruction of the data was done using the initial raw crystal data. This pass was done to reduce the background from channels such as $\pi^0\eta\eta$ and $\pi^0\pi^0\eta$, where there is a lost, low-energy gamma. By reducing the reconstruction thresholds, more of these background events could be positively identified by finding that lost gamma. Events were discarded if more than one π^0 or more than two η's were found, or if exactly two η's and one π^0 were found. This is intended to reduce that background from $\pi^0\eta\eta$ and $\pi^0\pi^0\eta$. For example, 47 % of the background from $\pi^0\eta\eta$ was discarded while only 12 % of the signal from $\eta(\omega \to \eta\gamma)$ was discarded (see table 4, cut 5, and figure 2).

After this second pass, the original reconstructed gammas were restored.

The π^0's and η's are detected in their two photon decay mode, and are therefore identified by their invariant mass, calculated by taking the invariant dot product of the sum of the 4-vectors of the two constituent gammas, or equivalently calculating

$$m_{ij} = \sqrt{2E_iE_j(1-\cos(\Theta))}.$$

The error of m_{ij}^2 is calculated using the errors of each gamma, in spherical coordinates $(E, \phi, \cos(\theta))_i$.

$$\frac{\sigma_{m_{ij}^2}}{m_{ij}^2}^2 = \left(\frac{\sigma_{E_i}}{E_i}\right)^2 + \left(\frac{\sigma_{E_j}}{E_j}\right)^2 + \left(\frac{\sigma_{\cos\Theta_{ij}}}{1-\cos(\Theta_{ij})}\right)^2$$

$$\cos\Theta_{ij} = \cos\phi_i \sin\theta_i \cos\phi_j \sin\theta_j + \sin\phi_i \sin\theta_i \sin\phi_j \sin\theta_j + \cos\theta_i \cos\theta_j$$

$$\sigma^2_{\cos\Theta_{ij}} = \sum_{k=i,j} \left(\frac{\partial \cos\Theta_{ij}}{\partial\phi_k}\sigma_{\phi_i}\right)^2 + \left(\frac{\partial \cos\Theta_{ij}}{\partial\theta_k}\sigma_{\theta_i}\right)^2$$

To satisfy the π^0 requirement, the $\gamma\gamma$ invariant mass must lie in a window of [85,185] MeV. This window is much wider than the experimental width of the π^0, but since unidentified π^0's form a significant portion of the the $\omega\rightarrow\eta\gamma$ background, the definition of a π^0 must be quite liberal in order to completely identify and thereby eliminate this form of background. To satisfy the η requirement, the $\gamma\gamma$ invariant mass squared must be near the η mass squared, $m_\eta = 547.45$, such that

$$\chi^2_{ij} = \left(\frac{m_{ij}^2 - m_\eta^2}{\sigma(m_{ij}^2)}\right)^2 < 3.$$

After a list of π^0's and η's was made, they were combined to form the following states, $\pi^0\pi^0\gamma$, $\eta\pi^0\gamma$ and/or $\eta\eta\gamma$ if possible. It is possible for an event to appear as more than one of these states simultaneously, and there may be more than one configuration to form a specific state.

The final chosen configuration was that which had the lowest value of

$$\chi^2 = \chi^2_a + \chi^2_b$$

where (a, b) is one of (π^0, π^0), (π^0, η) or (η, η).

	Cut		Number of Events (unnormalized)				
			Data	Monte Carlo Channel			
				$\pi^0\eta\eta$	$\pi^0\pi^0\eta$	$\eta(\omega\to\pi^0\gamma)$	$\eta(\omega\to\eta\gamma)$
•	0	Input	19,365,050	468,973	442,000	154,936	9,965
•	1	No tracks	17,332,428	442,308	405,317	145,200	9,402
•	2	Loose mom cut	11,220,582	363,720	337,806	120,825	7,802
•	3	5 gammas	1,012,827	38,618	47,042	84,973	5,828
•	4	4C χ^2 cut	618,525	20,443	25,129	63,365	4,383
∘	5	$N(\pi^0) \leq 1 \cap$ $N(\eta) \leq 2 \cap$ $\overline{\eta\eta\pi^0 + X}$	185,226	12,498	10,831	49,473	3,851
•	6	$N(\pi^0\pi^0\gamma) = 0$	142,569	12,156	9,563	45,788	3,775
•	7a	$N(\pi^0\eta\gamma) > 0 \cap$ $N(\eta\eta\gamma) = 0 \cap$ $E_{\gamma *} > 100$	92,919	1,939	5961	33,511	77
•	7b	$N(\eta\eta\gamma) > 0 \cap$ $N(\pi^0) = 0 \cap$ $E_{\gamma *} > 100$	1,240	3,073	0	8	1,837

Table 4
The event counts after sequential cuts. Cut 7 represents the final two channels, (7a) $\eta\pi^0\gamma$ and (7b) $\eta\eta\gamma$. •= Signal Enhancement Production, ∘= Background Suppression Production (see table 2). X in step 5 represents 0 or more additional particles.

The remaining unpaired gamma is labelled $\gamma_{\rm rad}$ for "radiated" to distinguish it from the others.

These particle identification windows were varied to check for systematic effects. The more interesting effect can be seen in figure 3, where the contributions from $\pi^0\pi^0\eta$ and $\eta(\omega\to\pi^0\gamma)$ fall quickly as the π^0 window is increased. The π^0 window of [85,185] was chosen because this suppresses those backgrounds sufficiently. See also section 5 for additional discussions of systematics.

Events with two or more π^0's were discarded in cut 6. Two groups were selected from the remaining events in cuts 7a and 7b.

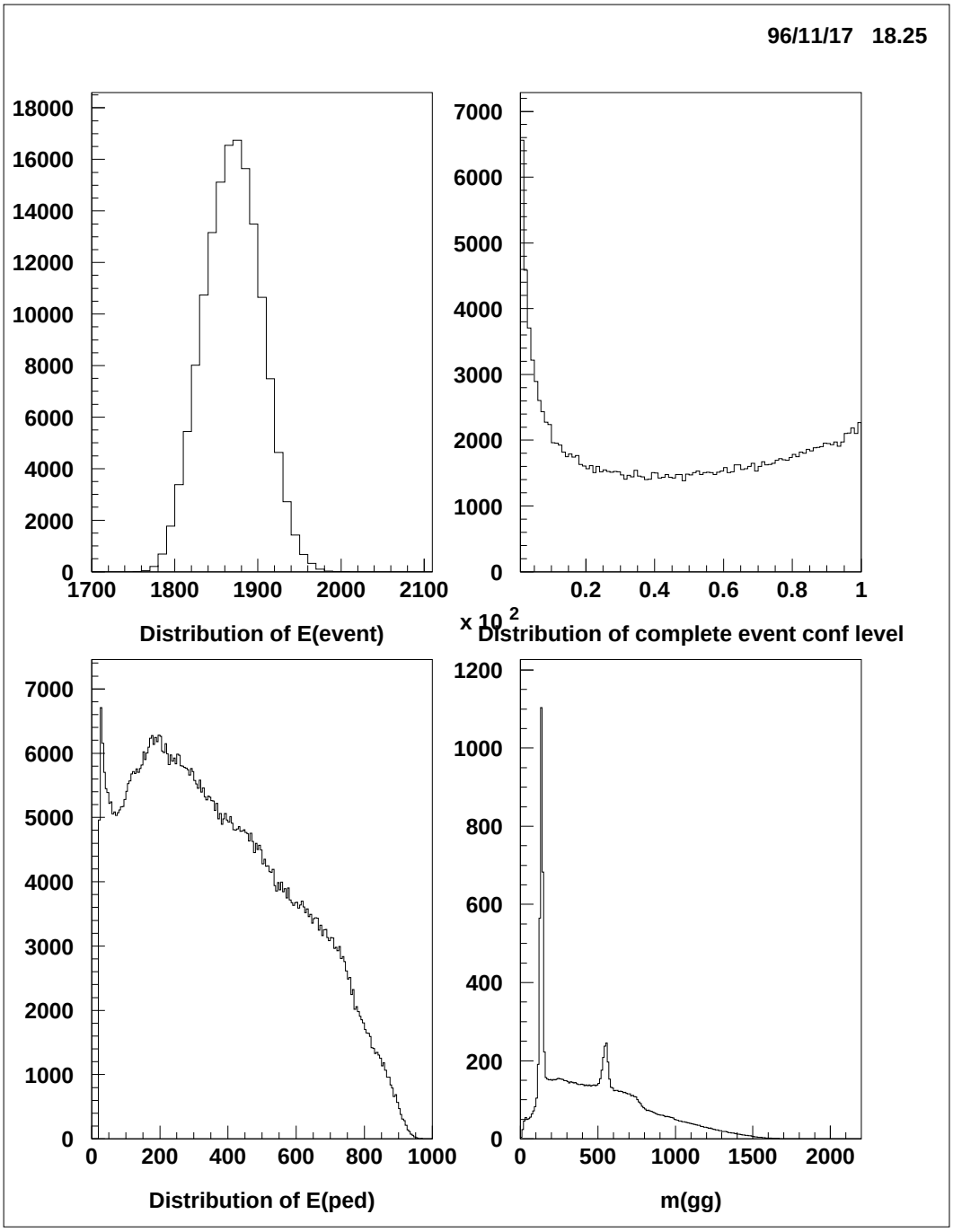

Fig. 1. Event quality after cut 4 (a) total Energy (b) 4C confidence level (c) PED energy (d) $\gamma\gamma$ invariant mass. Only a subset of the data is shown.

The $\eta\pi^0\gamma$ group, which is dominated by $\eta(\omega\rightarrow\pi^0\gamma)$, was selected with cut 7a:

(i) The number of $\pi^0\pi^0\gamma$ possible configurations is zero.
(ii) The number of $\eta\pi^0\gamma$ possible configurations is at least one.
(iii) The number of $\eta\eta\gamma$ possible configurations is zero.
(iv) $E_{\gamma_{\rm rad}} > 100$ MeV, to suppress split-off gammas.

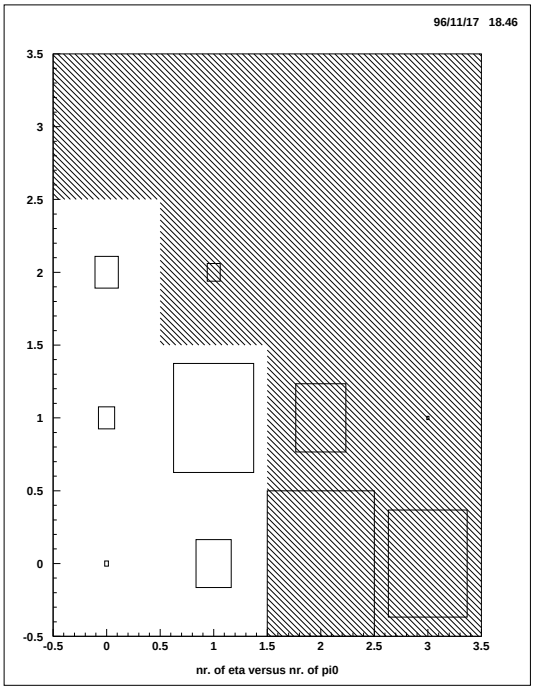

Fig. 2. Effect of background suppression cut 5. The number of π^0 and η's per event are plotted. The hatched region are events that are rejected. The events at $(x, y) = (1, 2)$ are background from $\pi^0\pi^0\eta$, while $(x, y) = (2, 1)$ are background from $\pi^0\pi^0\eta$.

The $\eta\eta\gamma$ group, which contains the desired channel $\eta(\omega{\rightarrow}\eta\gamma)$ was selected with cut 7b:

(i) The number of identified π^0's is zero.
(ii) The number of $\eta\eta\gamma$ possible configurations is at least one.
(iii) $E_{\gamma_{\rm rad}} > 100$ MeV, to suppress split-off gammas. (The $\omega{\rightarrow}\eta\gamma$ phase-space does not go below 100 MeV for $\gamma_{\rm rad}$).

In the later group, there are two η's. To distinguish these two, we used the fact that in the two body reaction 2, the initial two particles (η and ω) both have the unique momentum of 660 MeV/c. Thus, the η with momentum closest to 660 MeV was therefore called η_0 while the other was called η_ω, since in the desired signal, the latter η decays from ω. However, a tight cut on the momentum of η_0 around 660 MeV/c was not useful for this analysis. Due to the kinematic constraints imposed by all the cuts, this final cut would have forced the $\eta_\omega\gamma_{\rm rad}$ mass to be 781 MeV, which would have prevented the desired signal to be distinguished from the background.

In Fig 4, the invariant masses of the relevant identified particles are plotted for those events that pass the above cuts.

We refrained from using kinematic fitting because it would not have offered much to this analysis. Since this analysis was primarily a counting exercise, an

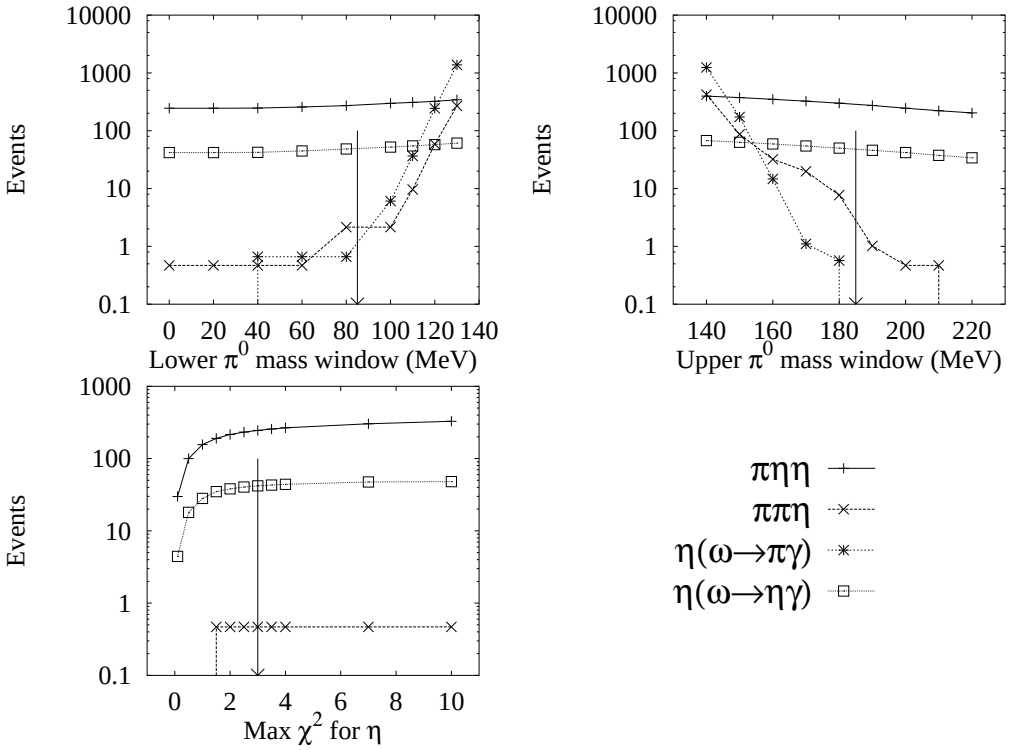

Fig. 3. The expected number of accepted events for the $\eta\eta\gamma$ group as a function of cut parameters, The chosen cut parameters are indicated with vertical arrows, and in each plot above, one cut parameter was varied while the others remained at the chosen values. Only a subset of the data is shown.

improvement in resolution (such as the omega width) would not have helped substantially. A 7C fit to the full state $\eta(\omega\rightarrow\eta\gamma)$ is counterproductive since it would then make the background indistinguishable from the signal.

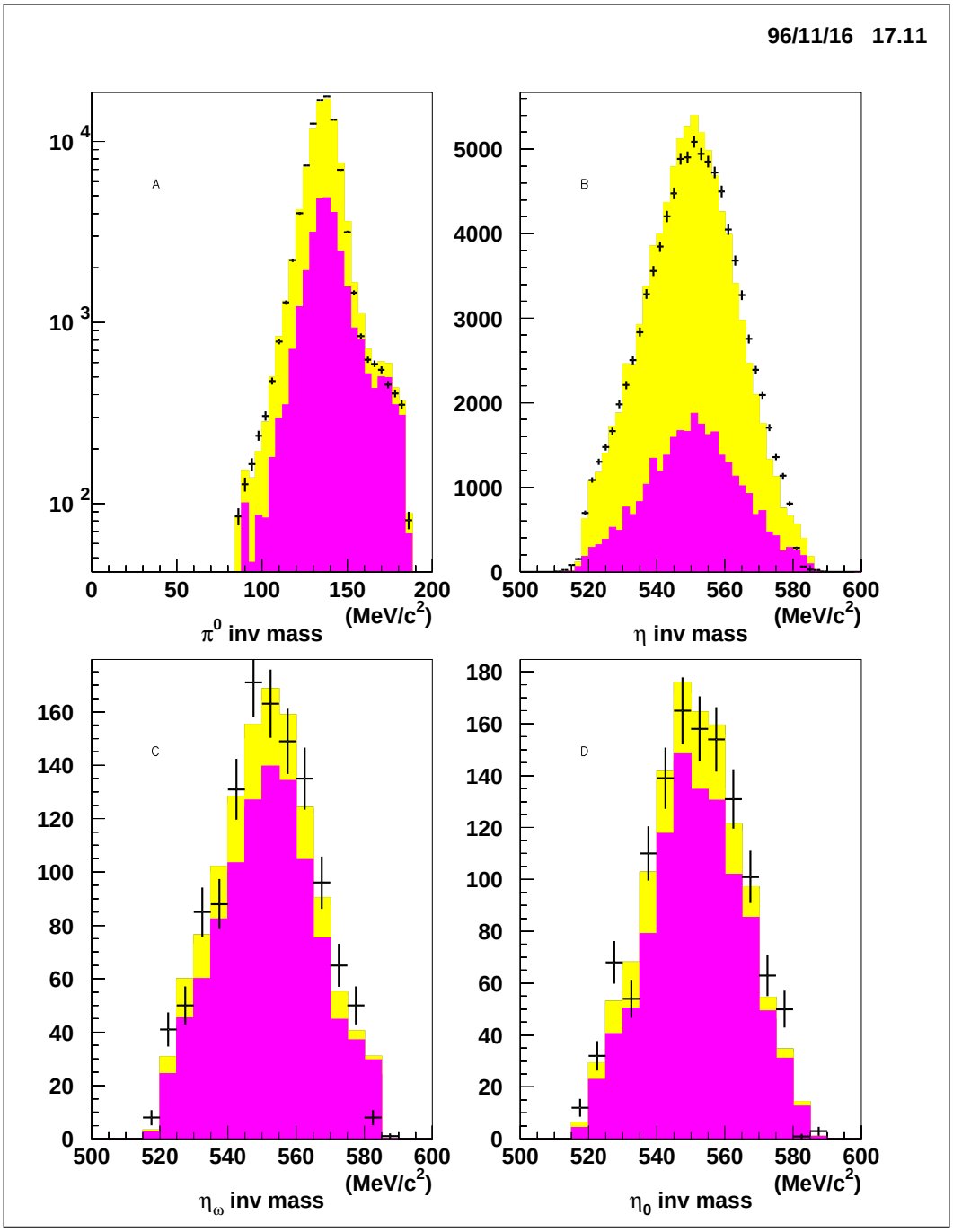

Fig. 4. Reconstructed invariant masses of π^0's and η's in $\eta\pi^0\gamma$ (**A** and **B**) and $\eta\eta\gamma$ (**C** and **D**) groups. The data are shown with error bars, while the shaded regions are expected contributions from individual channels, described in the text.

3 Background sources and Monte Carlo Simulations

There were three types of backgrounds with which we were concerned. Before we list them, we shall define "split-off" and "lost". A split-off describes a fake

gamma measurement that was not the result of a real gamma, but due to electro-magnetic shower fluctuations from another real gamma or other noise. This erroneously adds to the multiplicity of an event. A lost gamma describes a real photon that was ignored by the detection process, either by physically escaping the detector or not being identified by the reconstruction software as significant. Here we list the signal and background types along with the most significant channels of each.

(i) 4 gamma channels with 1 split-off to make 5 reconstructed gammas.
- $p\overline{p}\rightarrow\pi^0\pi^0+$ 1 split-off
- $p\overline{p}\rightarrow\eta\pi^0+$ 1 split-off
- $p\overline{p}\rightarrow\eta\eta+$ 1 split-off

(ii) 5 gamma channels.
- $p\overline{p}\rightarrow\eta(\omega\rightarrow\eta\gamma)$(signal channel)
- $p\overline{p}\rightarrow\pi^0(\omega\rightarrow\pi^0\gamma)$
- $p\overline{p}\rightarrow\eta(\omega\rightarrow\pi^0\gamma)$(signal channel and background for $\omega\rightarrow\eta\gamma$)
- $p\overline{p}\rightarrow\pi^0(\omega\rightarrow\eta\gamma)$(signal channel)
- $p\overline{p}\rightarrow\pi^0(\phi\rightarrow\eta\gamma)$
- $p\overline{p}\rightarrow\pi^0\rho^0$, $\rho^0\rightarrow\eta\gamma$ or $\rho^0\rightarrow\pi^0\gamma$
- $p\overline{p}\rightarrow\eta\rho^0$, $\rho^0\rightarrow\eta\gamma$ or $\rho^0\rightarrow\pi^0\gamma$

(iii) 6 gamma channels that lose 1 gamma to make 5 reconstructed gammas.
- $p\overline{p}\rightarrow\pi^0\pi^0\pi^0$, where one $\pi^0\rightarrow\gamma_{\rm rad}\gamma_{\rm lost}$
- $p\overline{p}\rightarrow\pi^0\pi^0\eta$, where one $\pi^0\rightarrow\gamma_{\rm rad}\gamma_{\rm lost}$
- $p\overline{p}\rightarrow\pi^0\eta\eta$, where the $\pi^0\rightarrow\gamma_{\rm rad}\gamma_{\rm lost}$
- $p\overline{p}\rightarrow\omega\omega$, each $\omega\rightarrow\pi^0\gamma$, where one $\pi^0\rightarrow\gamma_{\rm rad}\gamma_{\rm lost}$or one $\omega\rightarrow\pi^0\gamma_{\rm lost}$

Because of the strict cut on 4-momentum conservation, all split-offs or lost gammas must be of low enough energy to not significantly add to the total 4-momentum of the event, and thus are typically under 100 MeV. All of the 4 gamma channels (that is $\pi^0\pi^0$, $\pi^0\eta$ and $\eta\eta$) were effectively eliminated by requiring that the unmatched gamma (split-offs in these cases) have energy greater than 100 MeV. Events with ≤ 3 or ≥ 7 gammas did not appear to make any significant contribution to the 5 gamma channel, and were not considered.

The channels with $\rho^0\rightarrow\pi^0\gamma$ or $\rho^0\rightarrow\eta\gamma$ have net branching ratios as small as the desired $\eta(\omega\rightarrow\eta\gamma)$ channel, but due to the broad nature of the ρ^0, these channels were virtually indistinguishable from the broad $\pi^0\eta\eta$ background and hard to measure. However, the ρ^0 channel is important because it coherently adds to the ω channel. See the appendix in section 8 for a discussion.

The $\pi^0\pi^0\pi^0$ and $\omega\omega$ channels were also of low significance, i.e. their expected contributions to the data were smaller than the Poisson errors of the data. We have attempted including them in the fits, but their effect on the fit was insignificant, and therefore they were not included in any further analysis.

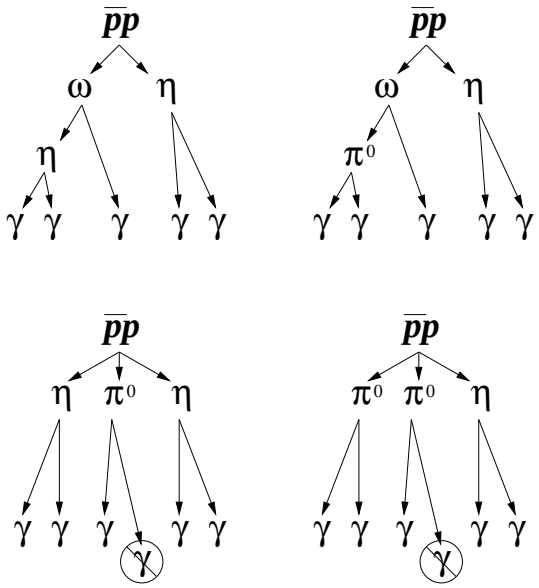

Fig. 5. Decay chain of four most important channels, the two signal channels $\eta(\omega\to\eta\gamma)$ (above left) and $\eta(\omega\to\pi^0\gamma)$ (above right), and the two background channels $\pi^0\eta\eta$ (below left) and $\pi^0\pi^0\eta$ (below right)

In the $\eta\pi^0\gamma$ group, there were primarily two contributing channels, the desired $\eta(\omega\to\pi^0\gamma)$ signal and the undesired $\pi^0\pi^0\eta$ background. The $\pi^0\eta\eta$ background makes a very small contribution.

In the $\eta\eta\gamma$ group, there were primarily four potentially contributing channels, the desired $\eta(\omega\to\eta\gamma)$ signal, the large broad $\pi^0\eta\eta$ background, the weaker broad $\pi^0\pi^0\eta$ background and the $\eta(\omega\to\pi^0\gamma)$ resonant background. Concerning $\eta(\omega\to\pi^0\gamma)$, $\omega\to\pi^0\gamma$ could appear to be $\omega\to\eta\gamma$ by misidentification of the 3 gammas, in which the real radiated gamma accidentally formed a fake η with one of two gammas from the π^0. This channel was indistinguishable from $\omega\to\eta\gamma$ in the sense that the three gamma invariant mass in both cases was m_ω. Unfortunately, the $\omega\to\pi^0\gamma$ channel was roughly 600 times stronger than the $\omega\to\eta\gamma$ channel, so a leakage of even 1% of the former would appear as a large signal in the later. It was due to this channel that the π^0 mass acceptance window ([85,185] MeV) was as wide as it was, to be sure to identify all π^0's, and therefore be able to cut against this channel. This π^0-anti-cut also eliminated $\pi^0\pi^0\eta$. The result was that only $\pi^0\eta\eta$ remained, and the broad nature of this channel allowed us to see the resonant ω peak above the background.

In all, there were four channels that needed to be well understood and simulated as accurately as possible using the Crystal Barrel version of the Monte Carlo (MC) program GEANT.

(i) $\pi^0\pi^0\eta$
(ii) $\pi^0\eta\eta$
(iii) $\eta(\omega\to\eta\gamma)$

(iv) $\eta(\omega \to \pi^0\gamma)$

The first two MC channels have been previously analyzed by the Crystal Barrel in detail[3]. Both Dalitz plots showed tremendous resonance structure, and thus the MC events needed to reflect this. The events were generated with a hit-or-miss phase space generator and thus were flat in phase space. The events were then weighted by their measured acceptance corrected Dalitz plots. This was done by binning the Dalitz plots, and normalizing the bins so that the average value of the (phase space allowed) bins was one.

Dalitz Plot	Events	Binning
$\pi^0\eta\eta$	395158	70 x 70
$\pi^0\pi^0\eta$	560834	90 x 90

For each MC event, the invariant masses of the primary particles was calculated, and then looked up in the normalized Dalitz plot. The corresponding bin value was used as the weighting of the event.

Both of these three pseudoscalar channels require many MC events to be generated, since the probability of an an accepted event of this type is very small. However, MC generation using the full detector simulation GEANT[6] is CPU demanding, and only a limited amount of statistics can be generated. To generate additional statistics, a simple, fast MC was done using the CERNLIB routine GENBOD[7] was used to generate 4-momenta of the gammas, for the channels $p\overline{p} \to \pi^0\eta\eta$ and $p\overline{p} \to \pi^0\pi^0\eta$. Only events with exactly one small energy photon that could be thrown away (i.e. 50 MeV or lower) were kept. The results were smeared with error gaussians that mimic the data, specifically,

$$\sigma(E) = 0.026E/\sqrt[4]{E/(1\text{GeV})}\text{MeV}$$

$$\sigma(\theta) = 0.025 \text{ rad}$$

$$\sigma(\phi) = 0.03 \text{ rad}$$

and the overall energies were scaled up by 0.488 % to account for the missing energy, so that the total energy of the GENBOD MC is the same as the GEANT MC after cut number 5. These events were then fed through the analysis procedure, starting just before cut number 6.

Both the GENBOD and CBGEANT simulations of the $\pi^0\eta\eta$ channel compared well. A calculation of the reduced χ^2 between the two gave a result of about 1.5. However, the GENBOD and CBGEANT simulations of the $\pi^0\pi^0\eta$ channel differ greatly. One is tempted to just ignore the simple, GENBOD simulation. However, the data does not prefer one over the other. For instance, in the $\eta\pi^0\gamma$

$\pi^0\pi^0\eta$	$\pi^0\eta\eta$	$\alpha(\pi^0\pi^0\eta)/$ $alpha(\eta(\omega\to\pi^0\gamma))$	$\alpha(\pi^0\eta\eta)/$ $\alpha(\eta(\omega\to\pi^0\gamma))$	$\alpha(\eta(\omega\to\eta\gamma))/$ $\alpha(\eta(\omega\to\pi^0\gamma))$
CBGEANT	CBGEANT	1.20 ± 0.01	0.87 ± 0.04	0.83 ± 0.09
GENBOD	CBGEANT	1.26 ± 0.01	0.90 ± 0.04	0.83 ± 0.09
CBGEANT	GENBOD	1.21 ± 0.01	0.87 ± 0.04	0.80 ± 0.09
Both	CBGEANT	1.25 ± 0.03	0.89 ± 0.04	0.83 ± 0.09

Table 5
Comparison of CBGEANT vs GENBOD simulations. "Both" means 49% CBGEANT, 51 % GENBOD, where both data sets were simultaneously fitted.

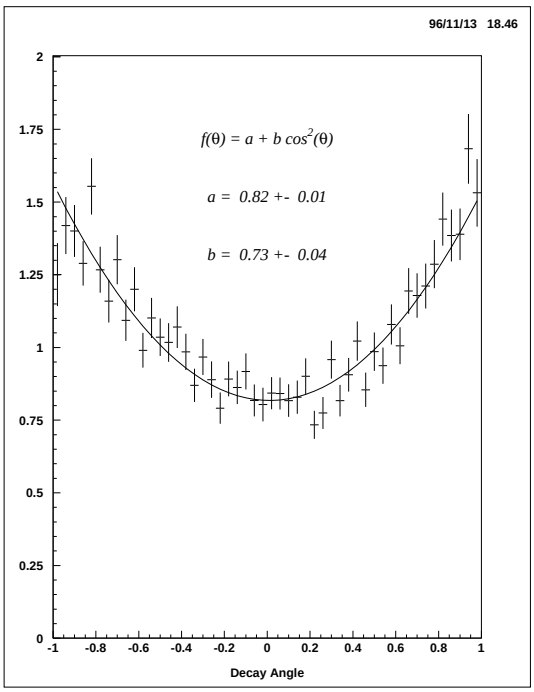

Fig. 6. The cosine of the Godfried/Jackson decay angle between $\gamma_{\rm rad}$ and the ω momentum direction, in the ω rest frame. The fitted curve is described in the text.

channel, the CBGEANT MC well describes the region of the $\pi^0\gamma$ invariant mass plot below 700 MeV, but has too few events to describe the region above 800 MeV. On the other hand, the GENBOD MC well describes the region above 800 MeV, but not below 700 MeV. To test the systematic effect of the different simulations, fits were performed using each or both. The GENBOD events were normalized to the CBGEANT events so that the final number of normalized events passing all cuts was the same for both.

Luckily, the answer is not very dependent on the choice of simulation, since this background is small and relatively flat under the strong ω peak.

The second two MC channels involve a decay of the form $V \rightarrow P\gamma$. It is observed that the ω does not decay isotropically in its rest frame, see figure 6 and appendix in section 7 for additional explanation. We used real data of the $\eta\pi^0\gamma$ channel, and selected events with $|M_{\pi^0\gamma} - M_\omega| < 20$MeV, histogramming the cosine of the angle between the γ and the ω momentum, in the rest frame of the ω. We then subtracted the estimated background contribution from $\pi^0\pi^0\eta$, divided by the corresponding flat MC efficiency histogram and then fitted the result with

$$f(\cos(\theta)) = a + b\cos^2(\theta).$$

The normalized fitted parameters (such that $\overline{f} = 1$) were $a = 0.77 \pm 0.01$ and $b = 0.69 \pm 0.03$. This function is then used to weight both the $\eta(\omega \rightarrow \pi^0\gamma)$ and the $\eta(\omega \rightarrow \eta\gamma)$ MC events, under the assumption that the angular dependence only depends on the J^{PC} quantum numbers, in which the η and π^0 are the same.

Some of the initial particles in the MC were specially defined, such that all ω's decayed radiatively and all η's were forced to decay to two gammas (normal BR = 38.8 %). Ideally, the number of MC events surviving all the cuts should have been at least an order of magnitude more than the number of data events surviving the cuts, in order to minimize unnecessary statistical errors due to low MC statistics. Unfortunately, we were limited to less than ideal MC statistics because of CPU speed. Nevertheless, for each channel, we have generated enough MC events so that after cuts, there were more MC events than data events. Table 6 summarizes the MC statistics.

The $\pi^0\eta\eta$ channel requires some addition comments, since it is the primary background to the desired channel. The channel appears as $\eta\eta\gamma$ when one of the gammas from the π^0 is lost. The loss of the π^0 gamma could have been due to several different processes.

(i) (about 40% of lost gammas) The lost gamma was of such small energy that it was ignored by the reconstruction software. The reconstruction software ignores all Particle Energy Depositions (PEDs) below a threshold, 20 MeV for the first pass and 4 MeV for the second pass. Gammas in the range of 5 to 50 MeV could appear as PEDs with energy below 20 MeV due to inefficiencies in the crystals. The energy of the lost gamma was small enough that there did not appear to have been any significant loss of energy in the event.

The problem with lowering the software energy threshold was that of split-offs. A gamma caused a shower of photoelectrons in the struck crystal which typically moved out and left behind energy in neighboring crystals. This collection of crystals was called a PED, and was assumed to have been triggered by one particle. However, sometimes the hit crystals

MC channel	Events	Net $p\overline{p}$ Branching Ratio*	Citation
$\pi^0\eta\eta$	468973	$(0.0020 \pm 0.0004) \times A^2$	[3]
$\pi^0\pi^0\eta$	442000	$(0.0082 \pm 0.0012) \times A$	[13]
$\eta(\omega\to\pi^0\gamma)$	154936	$(0.0151 \pm 0.0012) \times AB$	[8]
$\eta(\omega\to\eta\gamma)$	9965	$(0.0151 \pm 0.0012) \times A^2C$	[8]
$\rho^0\eta,\rho^0\to\eta\gamma$	925	$(0.0057 \pm 0.0015) \times A^2D$	[12]
$\eta\eta$	10000	$(0.000164 \pm 0.000010) \times A^2$	[8]
$\eta\pi^0$	10000	$(0.000212 \pm 0.000012) \times A$	[8]
$\pi^0(\omega\to\pi^0\gamma)$	1853	$(0.00573 \pm 0.00047) \times B$	[8]
$\omega\omega,\omega\to\pi^0\gamma$	4999	$(0.0332 \pm 0.00034) \times B^2$	[8]
$\pi^0\eta\omega,\omega\to\pi^0\gamma$	25000	$(0.0068 \pm 0.0005) \times AB$	[10]
$\omega(1420)\eta$	9863	?	
$a_1(1450)\eta$	980	?	
$\phi\eta$	9993	?	
$\phi\pi^0$	1000	?	

Table 6
Monte Carlo simulations. Number of events generated and overall branching ratio, where BR($\eta\to2\gamma$) $A = 0.388$, BR($\omega\to\pi^0\gamma$) $B = 0.085 \pm 0.005$, BR($\omega\to\eta\gamma$) $C = 0.00083 \pm 0.00021$, BR($\rho^0\to\eta\gamma$) $D = 0.00038 \pm 0.00007$

were not in a contiguous block, and the software identified these hit crystals (falsely) as two PEDs. Usually, one of the PEDs would have been of much lower energy than the other one, and these small energy PEDs were called split-offs. The number of split-offs per event rose dramatically if we lowered the minimum PED energy threshold, thus losing desired events.

(ii) (about 30% of lost gammas) The lost gamma merged with another gamma, forming only one PED. Since the energy of both gammas was accounted for, the total energy of the event was conserved, and the lost gamma could have a slightly higher energy (40-100 MeV). The shower masses of these were not significantly different from normal PEDs.

(iii) (about 20% of lost gammas) The low energy gamma was lost down the holes of the beam pipe.

(iv) (about 10% of lost gammas) Unknown cause.

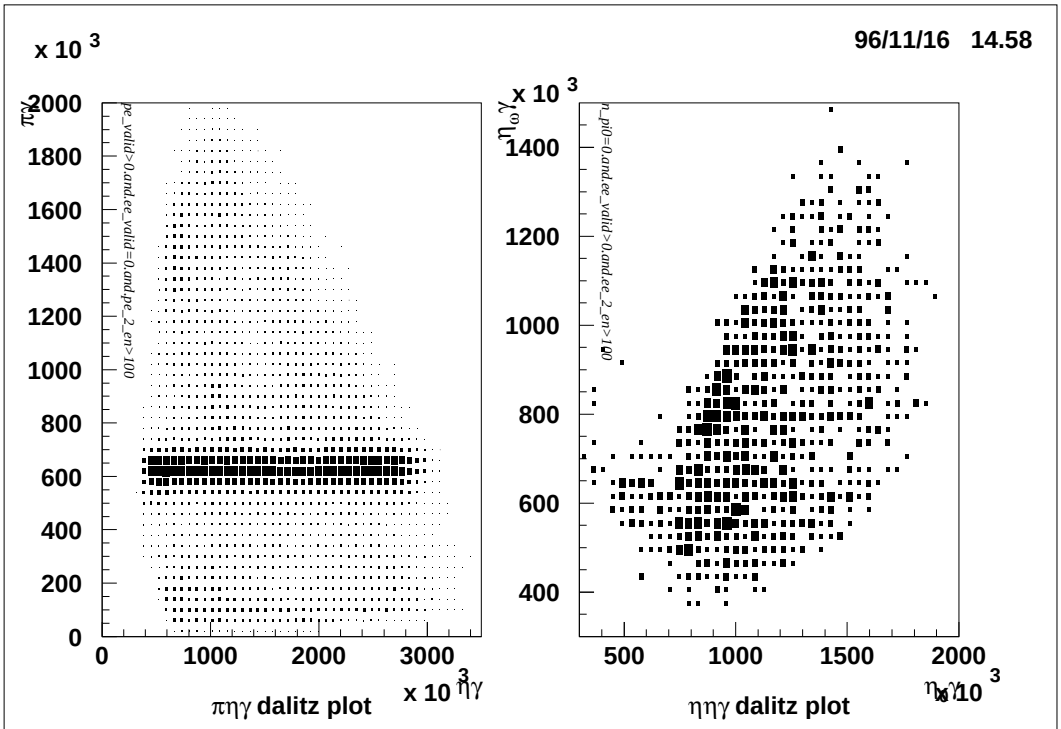

Fig. 7. Data Dalitz Plots, $\eta\pi^0\gamma$ at left and $\eta\eta\gamma$ at right. In all boxed histograms, the area of the box (as opposed to its perimeter) is directly proportional to the bin contents.

4 Fitting

The data was fitted against MC predictions, by binning the events in Dalitz plots,

(i) The $\eta\pi^0\gamma$ Dalitz plot, $M^2(\eta\gamma)$ vs. $M^2(\pi^0\gamma)$
(ii) The $\eta\eta\gamma$ Dalitz plot, $M^2(\eta_0\gamma)$ vs. $M^2(\eta_\omega\gamma)$

and using MINUIT to minimize the following log-likelihood function (for Poisson distributed data),

$$\chi^2 = \sum_i \left[2(N_i^{\rm mc} - N_i^{\rm data}) + 2N_i^{\rm data} \ln(N_i^{\rm data}/N_i^{\rm mc}) \right],$$

where $N_i^{\rm data}$ and $N_i^{\rm mc}$ are the observed (data) and theoretical (Monte Carlo) contents of the ith bin, i running over all bins of all histograms. The theoretical content of the ith bin is calculated as

$$N_{\rm mc}^i = \sum_{j=\text{MC channel}} T \frac{N_j^i(\alpha_j B_j)}{X_j}$$

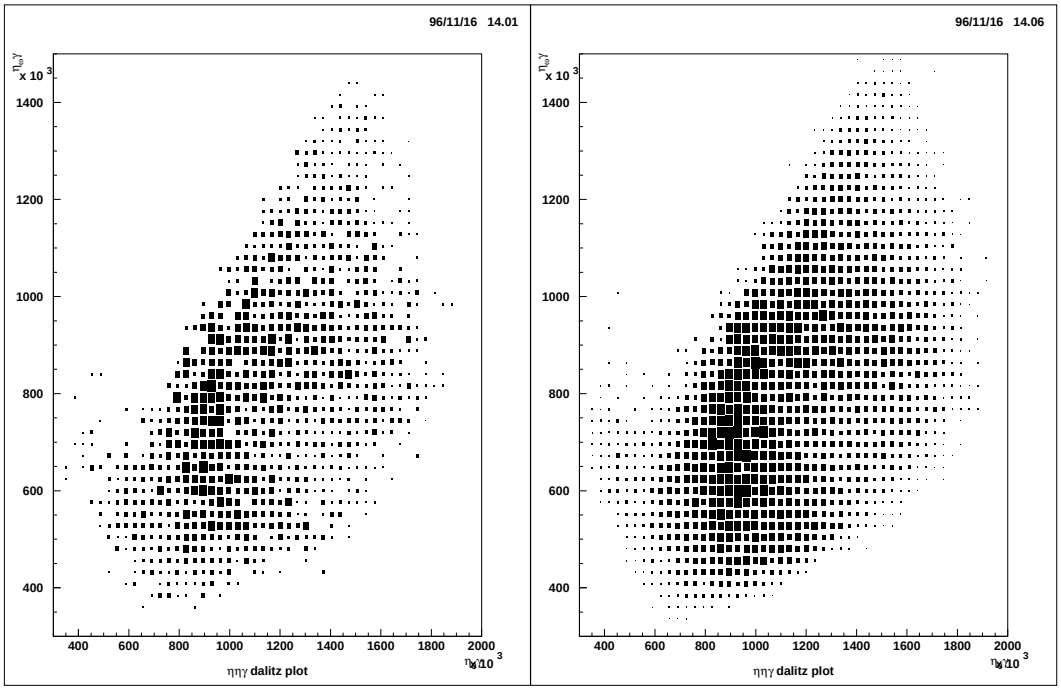

Fig. 8. $\eta\eta\gamma$ Dalitz plot for $\pi^0\eta\eta$ simulations, CBGEANT at left, GENBOD at right

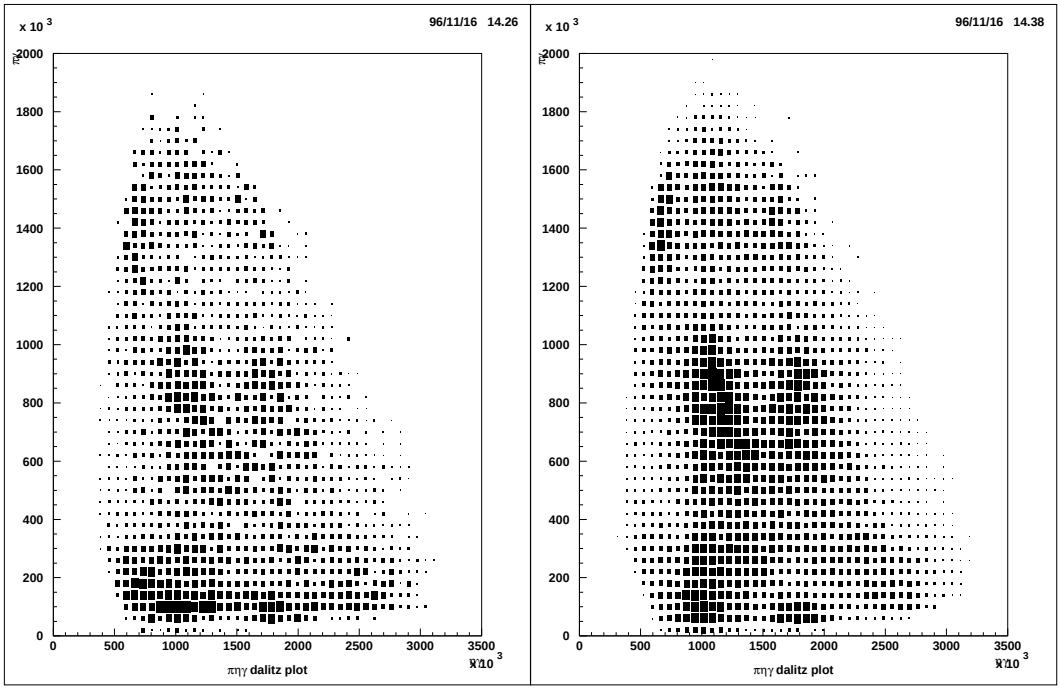

Fig. 9. $\eta\eta\gamma$ Dalitz plot for $\pi^0\pi^0\eta$ simulations, CBGEANT at left, GENBOD at right

where for each MC channel j. The values α_j are the normalization coefficients (unknown, but ideally unity), $T = 17,332,428/0.039$ is the total number of $p\overline{p}$ interactions derived from the number of all-neutral events, b_j is the branching ratio fixed to previously tabulated values, N_j^i is the number of surviving MC events in the ith bin, and X_j is the total number of MC events generated. Thus

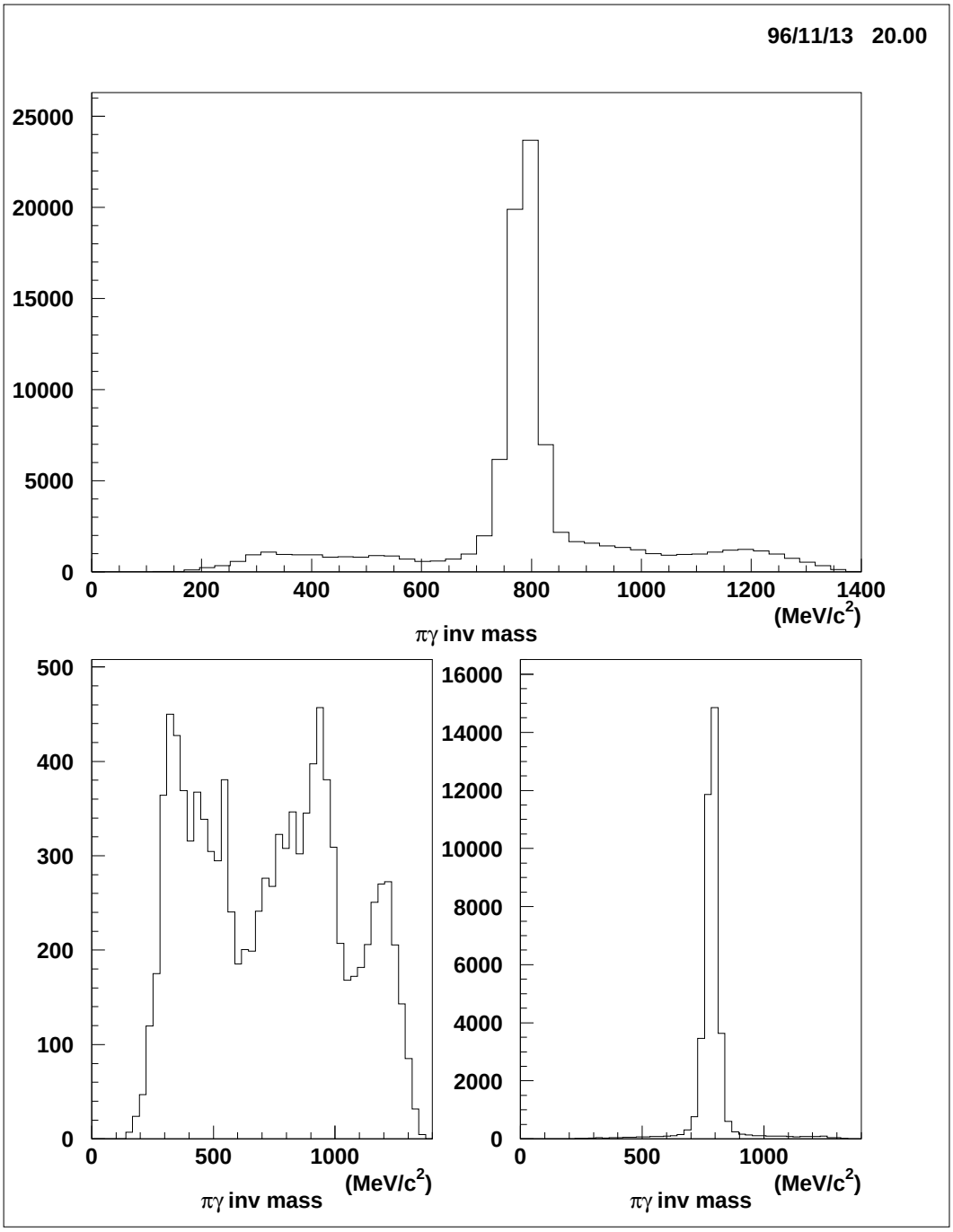

Fig. 10. Main components of the $\eta\pi^0\gamma$ Group, $\pi^0\gamma$ invariant mass. (Top) Data, (bottom left) $\pi^0\pi^0\eta$ MC, (bottom right) $\eta(\omega\to\pi^0\gamma)$ MC. The vertical scale of the MC distributions is in units of unnormalized MC events. See figure 11 for the fit.

the value of $(\alpha_j B_j)$ is the measured value of the branching ratio (from $p\overline{p}$) in this experiment. The bins on the perimeter of phase space were not corrected for (some of the bin lie outside of the physical region), but this should not be a significant effect in this analysis. The value of T is not well determined and does not include global trigger efficiencies, so only ratios of fit values α_j are

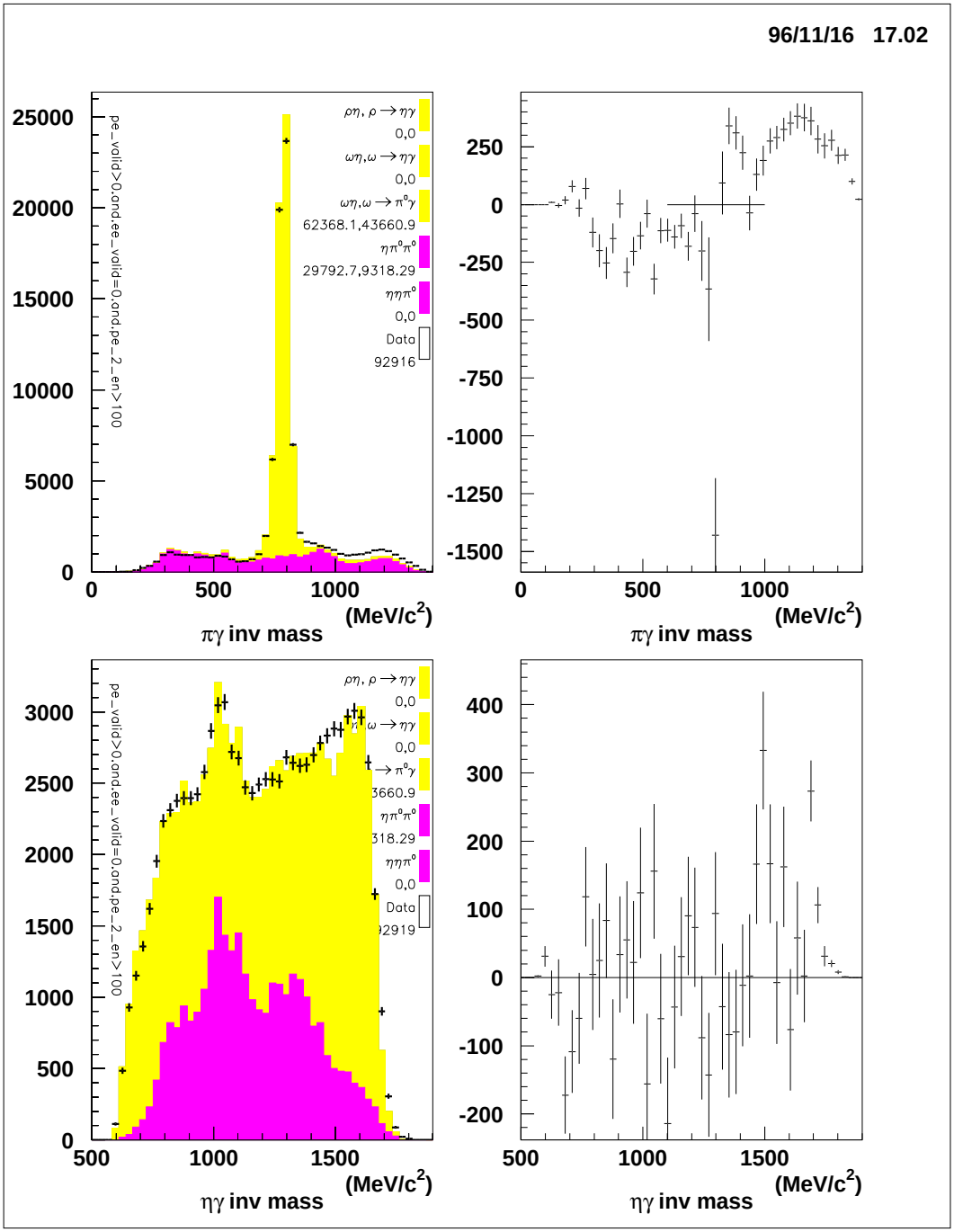

Fig. 11. Fit results of MC distributions (figure 10) to data in the $\eta\pi^0\gamma$ group, displayed as projections of the Dalitz plot. (Top) The $\pi^0\gamma$ invariant mass with difference plot at right. (Bottom) The $\eta\gamma$ invariant mass with difference plot at right. Error bars include both data and MC statistical errors. The data are shown with error bars. The shaded regions are contributions from various channels, derived from MC events. The light region is $\eta(\omega\to\pi^0\gamma)$, the dark region is background from $\pi^0\pi^0\eta$.

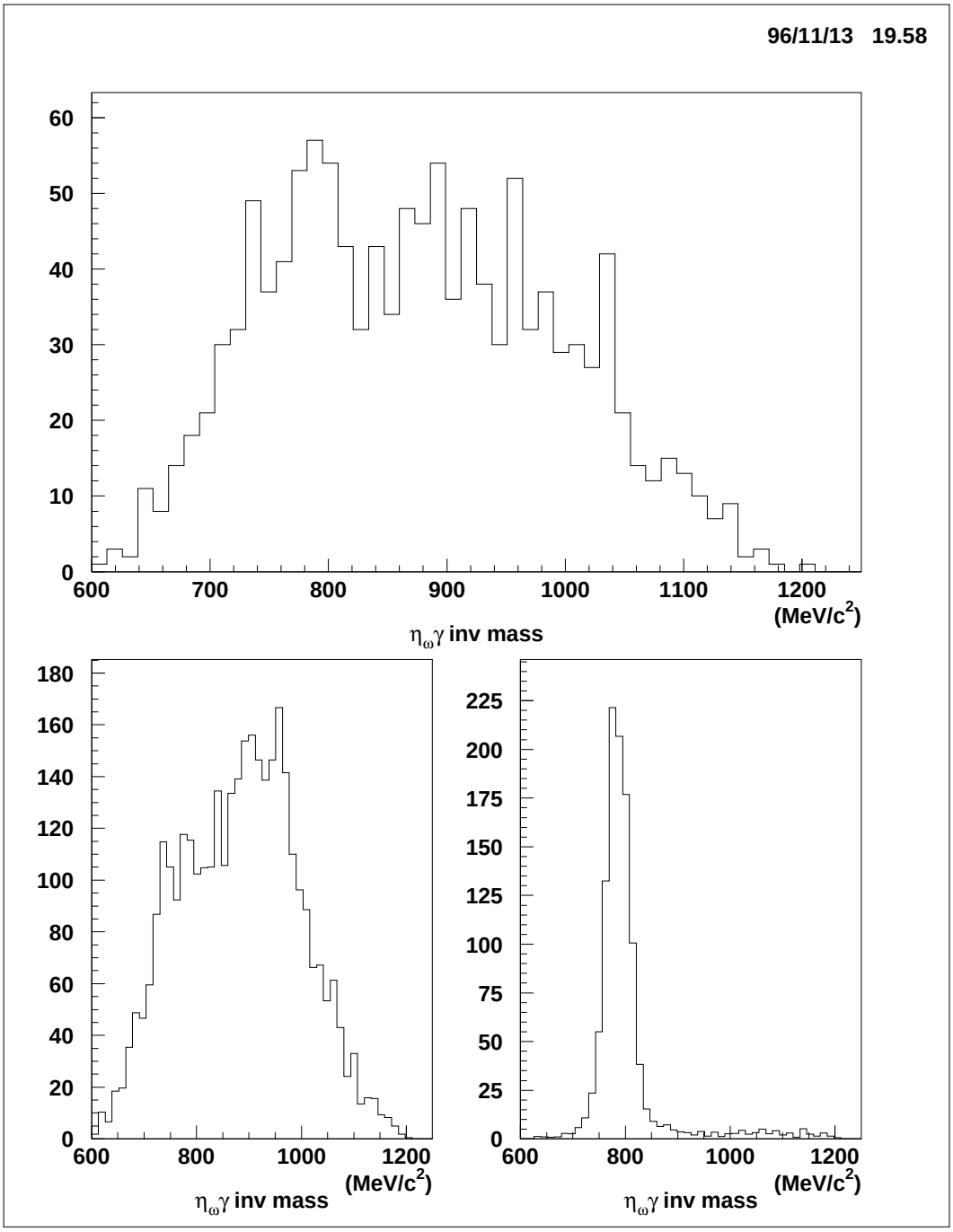

Fig. 12. Main components of the $\eta\eta\gamma$ Group, $\eta_\omega\gamma$ invariant mass. (Top) Data, (bottom left) $\pi^0\eta\eta$ MC, (bottom right) $\eta(\omega\to\eta\gamma)$ MC. The vertical scale of the MC distributions is in units of unnormalized MC events. See figure 13 for the fit.

meaningful, e.g. in comparisons between $\omega\to\eta\gamma$ and $\omega\to\pi^0\gamma$ the value of T cancels.

The α_j values are the free parameters of the fit. If all fit results are consistent with previously tabulated branching ratios, the values of α_j should be all the

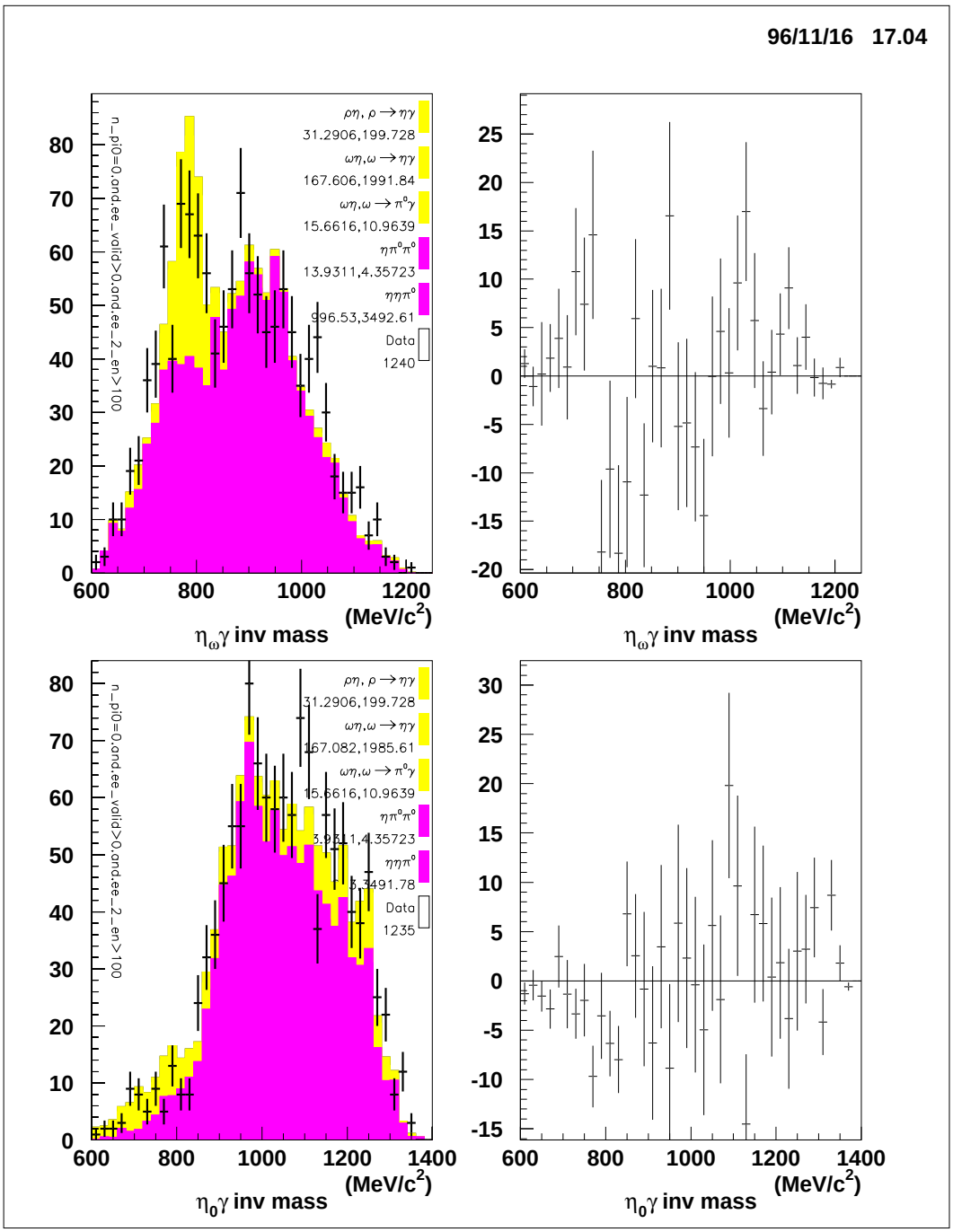

Fig. 13. Fit of MC distributions (figure 12) to data in the $\eta\eta\gamma$ group. (Top) The $\eta_\omega\gamma$ invariant mass with difference plot at right. (Bottom) The $\eta_0\gamma$ invariant mass with difference plot at right. Error bars include both data and MC statistical errors. The data are shown with error bars. The shaded regions are the contributions from various channels, derived from MC events: The light region is $\eta(\omega\rightarrow\eta\gamma)$, the dark region is background from $\pi^0\eta\eta$.

same. The results of the fits are shown in figures 11 and 13 as projections of the Dalitz plots.

The error estimates are due to

(i) *(stat)* The MINOS errors of the fit. This should include errors from the Poisson statistics of the data but not of the MC.
(ii) *(sys)* Systematic errors discussed in section 5

The results are summarized in table 7. The various errors are added in quadrature, and the net result is to be used only as a comparison of this experiment with the "best world average" which is defined to be equal to 1.0 for all channels. The ratio of $\pi^0\eta\eta$ to $\eta(\omega\to\pi^0\gamma)$ confirms previous measurements, while the ratio of $\pi^0\pi^0\eta$ to $\eta(\omega\to\pi^0\gamma)$ is higher and the ratio of $\eta(\omega\to\eta\gamma)$ to $\eta(\omega\to\pi^0\gamma)$ is lower (2 sigma from $(8.3 \pm 2.1) \times 10^{-4}$).

An interesting point is that the fit value for $\pi^0\pi^0\eta$ is more than one standard deviations from unity. This is either due to errors in the MC, an error in the $p\overline{p}\to\pi^0\pi^0\eta$ branching ratio, or due to the presence of another broad background channel. That there may be errors in the MC is indicated by the disparity in between the GENBOD simulation and the CBGEANT simulation.

The presence of a broad background seems unlikely due to the nice fit in figure 11, yet nevertheless is a plausible reason. We have eliminated the possibility of contamination because of the definition of the π^0, which had a [85,185] MeV $\gamma\gamma$ window. If we make the additional cut in the $\eta\pi^0\gamma$ group, requiring the π^0 to have mass [115,155] MeV, the $\pi^0\pi^0\eta$ fit factor does not change significantly (1.38 ± 0.03). Whether or not this excess is due to $\pi^0\pi^0\eta$ or not should not make a big difference on the answer for $\omega\to\eta\gamma$, since it is compared to $\omega\to\pi^0\gamma$, whose contribution is well constrained by the ω peak and not by the background ($\pi^0\pi^0\eta$ or other) underneath. We attempted using other poorly known resonances to describe the data, such as $a_1(1450)$ and $\omega(1420)$ decays into $\eta\gamma$. However the results were not convincing since both of these decays would have to have high branching ratios or the original particles would have to be produced copiously.

All measurements in this analysis are consistent with previous world averages, listed in the rightmost column of the table with their errors. The $\pi^0\pi^0\eta$ value is slightly too high, but this is likely due to the fact that the MC is not ideal, as seen in the comparison between GENBOD and CBGEANT simulations. However, the comparison also demonstrated that the exact form of the $\pi^0\pi^0\eta$ dalitz plot has little effect on the measurement on the important channel, i.e. $\eta(\omega\to\eta\gamma)$.

Channel	Fitted Events		Result ± Error		World Average
	$\eta\pi^0\gamma$	$\eta\eta\gamma$		± Stat. ± Sys.	(PDG + CB)
$\pi^0\eta\eta$	628	997	0.87	± 4 % ± 6%	1 ± 0.20
$\pi^0\pi^0\eta$	29793	14	1.20	± 1 % ± 7%	1 ± 0.12
$\eta(\omega\to\pi^0\gamma)$	62368	16	(1)	± 0.6% ± 1.4%	1 ± 0.10
$\eta(\omega\to\eta\gamma)$	7	168	0.83	± 11% ± 13%	1 ± 0.26
$\rho^0\eta$	2	31	1.05	± 40% ± –	1 ± 0.32
total	92798	1226			
data	92919	1241			

Table 7
Dalitz fit results and additional errors.

5 Systematics

5.1 Binning

The $\eta\eta\gamma$ Dalitz plot was binned in each of 20x20, 30x30, 40x40 and 50x50 two dimensional histograms. The variance of the $\eta(\omega\to\eta\gamma)$ fit due to binning was 5% which will be included in the systematic error, and there was no significant correlation with bin size.

5.2 MC Systematics

Shape of the MC distributions was assigned a 3% statistical error to be added to the measured BR. This error was assessed based on the difference between CBGEANT and GENBOD simulations.

5.3 π^0 and η Definitions

The π^0 window (nominally [85,185]) was varied over a large range to check the systematic dependence. This window is critical because a small window lets in a large background from $\eta(\omega\to\pi^0\gamma)$. The results are plotted in figure 14, where one can see that the number of background events changes dramatically, but the fit values remain constant. The systematic errors of the fit values are based on the RMS variation of the fit values. The η window was also varied with little change in the fit values.

	$\eta(\omega\to\eta\gamma)$ events		$\pi^0\eta\eta$ events	
	Dalitz	Proj.	Dalitz	Proj.
Fake #1	172 ± 22	138 ± 23	980 ± 37	954 ± 36
Fake #2	175 ± 21	163 ± 20	967 ± 37	956 ± 31
Fake #3	157 ± 18	107 ± 19	1012 ± 39	929 ± 36
Average Fake	168 ± 8	136 ± 23	986 ± 19	946 ± 12
Should be	168	168	997	997

Table 8
Comparison between Dalitz fitting and Projection fitting using fake (known) data.

5.4 Tabulated BR's

The BR($p\overline{p}\to\omega\eta$) cancels for the final result. The PDG error of BR($\eta\to\gamma\gamma$) is negligible, while the error of BR($\pi^0\to\gamma\gamma$) is 0.8% (see PDG [14]).

5.5 Dalitz plot fit vs. Projection fit

We note that the projection in figure 13 appears to be a poor fit, that is the fitted contribution of $\eta(\omega\to\eta\gamma)$ appears significantly higher than the data allows. We believe that this is an unfortunate consequence of the projection of the Dalitz plot with low statistics.

In order to test this hypothesis, we generated 3 fake data sets that contained exactly 352 $\eta(\omega\to\eta\gamma)$ events and 4054 $\pi^0\eta\eta$ events that survived cuts 1-5. These events continued through the cut procedure and treated just like the real data. On average, in each of these fake data sets, there should be 168 events of type $\eta(\omega\to\eta\gamma)$ and 997 events of type $\pi^0\eta\eta$ identified by the fit, which are the values found in the fit to real data. A fit using the Dalitz plot and a fit using the two projections was done for each fake data set, see table 8. The Dalitz fit is clearly better, since the averages match the expect value perfectly (100% and 99% of the correct value of $\eta(\omega\to\eta\gamma)$ and $\pi^0\eta\eta$,respectively) and the scatter of each fit around this average is small, compared to the values from the projection fits, which are significantly too small (80% and 95% of the correct values of $\eta(\omega\to\eta\gamma)$and $\pi^0\eta\eta$, respectively) and suffer from larger variance in the fit values for $\eta(\omega\to\eta\gamma)$. No additional systematic error is added therefore for using the Dalitz plot fit.

Systematic	Est. Error of Fit Value (α)			
	$\pi^0\eta\eta$	$\pi^0\pi^0\eta$	$\eta(\omega\to\pi^0\gamma)$	$\eta(\omega\to\eta\gamma)$
π^0 window	3%	2%	0.7%	9%
η window	3%	1%	0.3%	6%
MC statistics	1.7%	1.0%	0.5%	2.2%
MC systematics	3%	3%	3%	3%
BR($\eta\to\gamma\gamma$)*	0.8%	–	–	0.8%
Dalitz Binning	3%	4%	1%	6%
Net Error	6%	7%	1.4%	13%

Table 9
The estimated systematic errors. * indicates error relative after dividing by measured BR($\eta(\omega\to\pi^0\gamma)$). ($\rho^0\eta$ is not included since the statistical errors were enormous.)

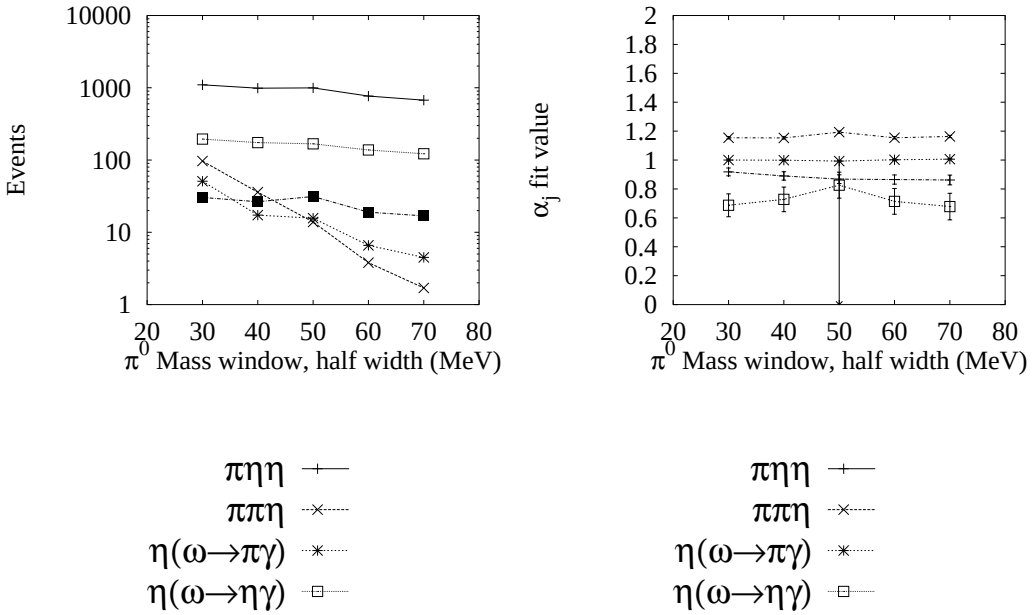

Fig. 14. Variation of Dalitz plot with changes in π^0 window. The x-axis is the half width of the π^0 window in MeV. (a) The number of accepted events of each type (b) The fit results (α_j).

5.6 Non-uniform background in $\eta\eta\gamma$

The $\pi^0\eta\eta$ background had much Dalitz plot structure, and many events were concentrated in certain areas. One such cut that reduced the background more than the signal was cutting on the angle between the radiated gamma and η_ω, in the ω center-of-mass frame. The distribution was symmetric about 0 for the $\eta(\omega\to\eta\gamma)$ signal ($1+\cos^2\theta$ distribution), but highly skewed to values greater than 0 (forward direction) for the $\pi^0\eta\eta$ background (see figure 15 (a). As seen in figure 15 (b,c,d), the fit results from the Dalitz plot appear better as $\cos\theta$ goes towards -1.0, where the background from $\pi^0\eta\eta$ is much reduced. This shows that the Dalitz fit is more sensitive to the signal in the regions were the $\pi^0\eta\eta$ background is smallest.

5.7 ρ^0 interference

We discuss ρ^0 interference in the appendix, section 8. The approximations made here are quite good, and have systematic errors on the order of 1%. There is an additional error based on the error of the phase between the ρ^0 and the ω amplitudes. The correction coefficient is $C(-18^\circ) = 0.90^{+0.10}_{-0.12}$. This systematic error is included at the end.

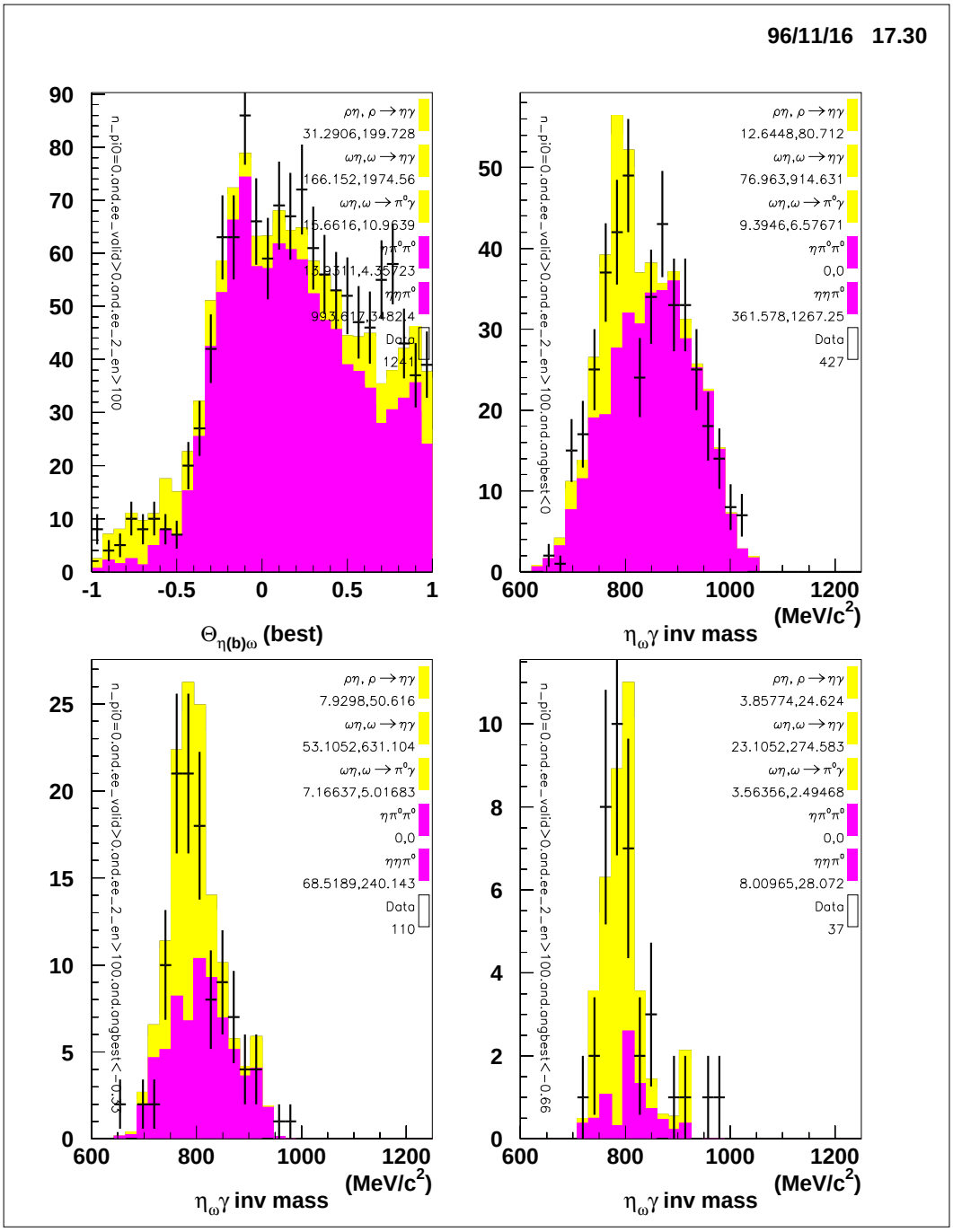

Fig. 15. (a) The distribution of $\cos\theta$ of the Godfried-Jackson decay angle. The other three histograms are the same $\eta\gamma$ invariant mass plots of figure 13 but with cuts on this angle. (b) $\cos\theta < 0$ (c) $\cos\theta < -.33$ (d) $\cos\theta < -.66$

6 Conclusion

The result from the fit is

$$\frac{\mathrm{BR}(\omega\to\eta\gamma)}{\mathrm{BR}(\omega\to\pi^0\gamma)} = \left(\frac{\mathrm{BR}(\omega\to\eta\gamma)}{\mathrm{BR}(\omega\to\pi^0\gamma)}\right)_{\mathrm{PDG}} \times \left(\frac{\alpha(\omega\to\eta\gamma)}{\alpha(\omega\to\pi^0\gamma)}\right)_{\mathrm{fit}} \tag{5}$$

$$= \left(\frac{8.3\times10^{-4}}{8.5\times10^{-2}}\right)_{\mathrm{PDG}} \times \left(\frac{0.83\pm.09\pm.11}{1\pm.006\pm.014}\right)_{\mathrm{fit}} \tag{6}$$

$$= (8.1\pm0.9\ (\mathrm{stat})\pm1.1\ (\mathrm{sys}))\times10^{-3}. \tag{7}$$

Using the correction coefficient for the incoherent assumption (appendix, section 8), $C(-18^\circ) = 0.90^{+0.10}_{-0.12}$

$$\frac{\mathrm{BR}(\omega\to\eta\gamma)}{\mathrm{BR}(\omega\to\pi^0\gamma)} = (7.3\pm0.8\ (\mathrm{stat})\pm1.2\ (\mathrm{sys}))\times10^{-3}$$

Using the PDG value for $\mathrm{BR}(\omega\to\pi^0\gamma)$, we get

$$\boxed{\mathrm{BR}(\omega\to\eta\gamma) = (6.2\pm0.7_{\mathrm{stat}}\pm1.0_{\mathrm{sys}})\times10^{-4}}$$

We also arrive at a value for $\mathrm{BR}(\rho^0\to\eta\gamma)$, where the large error comes from the fit and from the $\mathrm{BR}(p\overline{p}\to\rho^0\eta)$,

$$\mathrm{BR}(\rho^0\to\eta\gamma) = (4.0\pm2.0)\times^{-4}.$$

Various theories and measurements are summarized in table 10.

Table 10
Theoretical Predictions (top) and Previous Measurements (bottom)

Reference	*Model or ω source*	BR($\omega\to\eta\gamma$) $[10^{-4}]$	BR($\rho^0\to\eta\gamma$) $[10^{-4}]$
Zhong[15] **	Exact SU(3)	10.1	
Zhong[15] **	Broken SU(3)	5.2	
Benayoun[16]	Model "1"	6.14 ± 0.58	
	Model "2"	3.27 ± 0.44	
Barik[17]	Set "1"	6.5	
	Set "2"	6.76	
	Static	5.8	
Singer[18]	Cloudy Bag	2.7	
Zhong[15]	M1 Cloudy Bag	3.1 – 3.3	
Bramon[19]	Broken SU(3)	6.1 ± 0.7	
Dolinksy[20]	$e^+e^-\to\omega$	$6.4^{+7.0}_{-4.7}$	
	4.0 ± 1.1 (+)		
Alde[21]	$\pi^- p\to\omega n$	8.3 ± 2.1	–
This measurement	$p\overline{p}\to\omega\eta$	(6.2 ± 1.2)	4.0 ± 2.0

References

[1] P.J. O'Donnel, "Radiative decays of mesons," *Rev. Mod. Phys* **53** (1981) 673.

[2] Crystal Barrel Collaboration, E. Aker, *et al.*, "The Crystal Barrel: Meson Spectroscopy at LEAR with a 4π Neutral and Charged Detector," *Nucl. Instr. & Meth.* **A321** (1992) 69.

[3] Crystal Barrel Collaboration, C. Amsler, *et al.*, "Coupled channel analysis of $p\overline{p}$ annihilation into $\pi^0\pi^0\pi^0$, $\pi^0\eta\eta$, and $\pi^0\pi^0\eta$." *Physics Letters* **B355** (1995) 425.

[4] *Physics Letters* **B311** (1993) 371.

[5] Crystal Barrel Collaboration, C. Amsler, *et al.*, "Antiproton-proton annihilation at rest into $\omega\pi^0\pi^0$," *Physics Letters* **B311** (1993) 362.

[6] R. Brun, *et al.*, Internal Report CERN DD/EE/84-1, CERN, 1987.

[7] F. James, *N-Body Monte-Carlo Event Generator*, Program Library W515, CERN, 1975.

[8] Crystal Barrel Collaboration, C. Amsler, *et al.*, "Antiproton-proton annihilation at rest into two-body final states," *Z.Phys* **C58** (1993) 175.

[9] *Zeit.Phys.* **A351** (1995) 325.

[10] Crystal Barrel Collaboration, C. Amsler, *et al.*, "Study of $p\overline{p}$ annihilation at rest into $\omega\eta\pi^0$," *Physics Letters* **B327** (1994) 425.

[11] R. Bizzari *et al.*, *Nucl. Phys.* **B14** (1969) 169.

[12] C. Amsler and F. Myhrer, "Low Energy Antiproton Physics," *Annu. Rev. Nucl. Part. Sci.* **41** (1991) 235.

[13] Crystal Barrel Collaboration, C. Amsler, *et al.*, "Study of $f_0(1500)$ decays into 4 π^0's in $p\overline{p}$ annihilations into five π^0's at rest" *Physics Letters* **B380** (1996) 453.

[14] Particle Data Group, *Phys. Rev.* **D50** (1994) 1196.

[15] Y.S. Zhong, T.S. Cheng, A.W. Thomas, "The M1 radiative decay of low-lying mesons in the cloudy bag model with centre-of-mass correction," *Nucl. Phys.* **A559** (1993) 579.

[16] M. Benayoun, Ph. Leruste, L. Montanet, J.-L. Narjoux, "Meson Radiative Decays and Anomaly Physics, a Test of QCD," LPC-94-31, June 30 ,1994.

[17] N. Barik, P.C. Dash, "Radiative decay of light and heavy mesons," *Phys. Rev.* **D49** (1994) 299.

[18] P. Singer, G.A. Miller, *Phys. Rev.* **D39** (1989) 825.

[19] A. Bramon, A. Grau, G. Pancheri, "Radiative vector-meson decays in SU(3) broken effective chiral Lagrangians," *Phys. Lett.* **B344** (1995) 240.

[20] S. Dolinsky, *et al.*, "Radiative decays of ρ^0 and ω mesons," *Z.Phys* **C42** (1989) 511.

[21] IHEP-PPLA-LANL-INRU Collaboration D. Alde, *et al.*, *Phys. At. Nucl.* **56** (9), September 1993, 1229. *Z. Phys.* **C61** (1994) 35.

[22] *Physics Letters* **B322** (1994) 431.

[23] Claudio Pietra, "Rare radiative ω decays", Crystal Barrel Technical Report, August 1996.

7 Appendix: Polarized Decay

In general, a polarized spin particle will not decay isotropically. For spin-1 particles decaying into spin-0 particles, the following radiation partterns are observed:

$$|1 \pm 1\rangle = \tfrac{1}{2}(1 + \cos^2\theta) \tag{8}$$

$$|00\rangle = \sin^2\theta \tag{9}$$

Annihilations of $p\overline{p}$ occur primarily in low angular momentum states, written in ${}^{2s+1}L_J^{(PC)}$ format:

$${}^1S_0^{(-+)}, {}^3S_1^{(--)}, {}^1P_1^{(+-)}, {}^3P_0^{(++)}, {}^3P_1^{(++)}, {}^3P_2^{(++)}$$

When decaying into vector + pseudoscalar, i.e. $p\overline{p}\rightarrow\omega\eta$ or $p\overline{p}\rightarrow\omega\pi^0$, only ${}^3S_1$ and ${}^1P_1$ states are allowed by C-parity.

In the frame of the vector particle, the orbital angular momentum quantized along the motion axis of the vector particle always has $m_L = 0$, because $\vec{L}\cdot\vec{P} = (\vec{R}\times\vec{P})\cdot\vec{P} = 0$.

Annihilation	Vector+Pseudoscalar System		
	J^{PC}	Orbital Ang. Mom. $\|Lm\rangle$	Spin Ang. Mom. (S)
${}^1P_1$	1^{+-}	$\|00\rangle$	1
${}^3S_1$	1^{--}	$\|10\rangle$	1
${}^1P_1$	1^{+-}	$\|20\rangle$	1

We now examine the Clebsch-Gordan coefficients to couple $L + S = J$, where $J = 1$ in all cases.

$\langle LSm_Lm_s\|Jm_J\rangle$	value
$\langle 01\ 0\ 0\|1\ 0\rangle$	1
$\langle 11\ 0\ +1\|1\ +1\rangle$	$-\sqrt{1/2}$
$\langle 11\ 0\ 0\|1\ 0\rangle$	0
$\langle 11\ 0\ -1\|1\ -1\rangle$	$\sqrt{1/2}$
$\langle 21\ 0\ +1\|1\ +1\rangle$	$\sqrt{1/10}$
$\langle 21\ 0\ 0\|1\ 0\rangle$	$-\sqrt{2/5}$
$\langle 21\ 0\ -1\|1\ -1\rangle$	$\sqrt{1/10}$

Finally, the radiation distributions are as follows, obtained by multiplying the pure polarization distributions by the C-G coefficients squared and summing, then renormalizing to the form $1 + b\cos^2\theta$.

$p\overline{p}$	V+P System	Radiation Distribution
$^1P_1$	$L = 0$	1 (isotropic)
$^3S_1$	$L = 1$	$1 + \cos^2\theta$
$^1P_1$	$L = 2$	$1 - 3/5\cos^2\theta$

For antiproton annihilations in liquid hydrogen, the ratio of P to S wave annihilation has been measured in other experiments with values ranging from 0 to 10%, while in gaseous hydrogen annihilation it is closer to 50%. In this measurement of $\omega \to \pi^0\gamma$ decays, the decay angle distribution is consistent with mostly S-wave annihilation.

8 Appendix: Coherent vs Incoherent Assumptions

The amplitude which describes the production of ρ^0 and ω and subsequent decays into $\eta\gamma$ is a coherent sum of the two individual amplitudes. Our final branching ratio measurement of $\omega\to\eta\gamma$ should be independent of any contribution from ρ^0. Simply counting the ω's in the $\eta\gamma$ invariant mass plot is *not* correct, because the number of events in this peak has been modified by the addition of extra pseudo-omega events which are in reality the consequence of the crossterms of the ρ^0 and ω amplitudes.

Consider the norm-squared of the total amplitude,

$$|S|^2 = |S_\omega + e^{i\phi} S_\rho|^2 \tag{10}$$

where

$$S_x = \frac{|A_x||T_x|}{m - m_x + i\Gamma_x/2}$$

and

$$|A_x| = \sqrt{BR(p\overline{p}\to x\eta)}$$

$$|T_x| = \sqrt{BR(x\to\eta\gamma)\Gamma_x}$$

where $x = \omega$ or $x = \rho^0$. We have neglected direct ρ^0-ω mixing through off-diagonal elements of the mass matrix, because it has little effect on this measurement.

However, we have assumed in the fit that the channels are *incoherently* summed. It turns out that this assumption, while technically incorrect, still leads to meaningful results. Consider the incoherent summation,

$$I^2 = |S_\omega|^2 + |S_{\rho^0}|^2 \tag{11}$$

The difference between the two assumptions is the presence of the cross term,

$$|S|^2 - I^2 = S_\omega\, e^{-i\phi} S^*_{\rho^0} + S^*_\omega e^{i\phi} S_{\rho^0}.$$

However, because the ρ^0 is so broad, to a good approximation, we can write,

$$I^2 \doteq C(\phi)\ |S|^2$$

over the range of the ω peak, where $C(\phi)$ is a correction factor calculated by integrating each side over the ω peak,

$$C(\phi) = \left(\int_{m=761}^{801} I^2 d\,m \right) / \left(\int_{m=761}^{801} |S|^2 d\,m \right),$$

using the tabulated values

$$BR(p\overline{p}\rightarrow\omega\eta) = (1.51 \pm 0.12) \times 10^{-2} \quad (12)$$
$$BR(p\overline{p}\rightarrow\rho^0\eta) = (5.7 \pm 1.5) \times 10^{-3} \quad (13)$$
$$BR(\omega\rightarrow\eta\gamma) = (8.3 \pm 2.1) \times 10^{-4} \quad (14)$$
$$BR(\rho^0\rightarrow\eta\gamma) = (3.8 \pm 0.7) \times 10^{-4} \quad (15)$$

for A_x and T_x. In other words, the form of the coherent amplitude squared is (somewhat coincidentally) proportional to the incoherent amplitude squared. This allows us to fit the data using an incoherent assumption, and then scale the measuresult for BR($\omega\rightarrow\eta\gamma$) by C to arrive at the true independent branching ratio, free from the influence of ρ^0.

We find $C(0) = 0.85$, $C(-18°) = .91$, and $C(\pi) = 1.22$, see figure 16. The additional systematic error due to this approximation is only 1%. (One may iterate this calculation of $C(\phi)$ using a value for the branching ratio [2] $BR(\omega\rightarrow\eta\gamma) = 6.4\times10^{-4}$, and get $C(0) = .83$, $C(-18°) = .90$ and $C(\pi) = 1.25$, thus this correction is not very sensitive to the exact branching ratios.)

As measured in [23], $\phi = (-18^{+58}_{-27})°$. This translates to a correction coefficient of $C(-18°) = 0.90^{+0.10}_{-0.12}$. This error is included at the end.

[2] An average between this result and the result from [23]

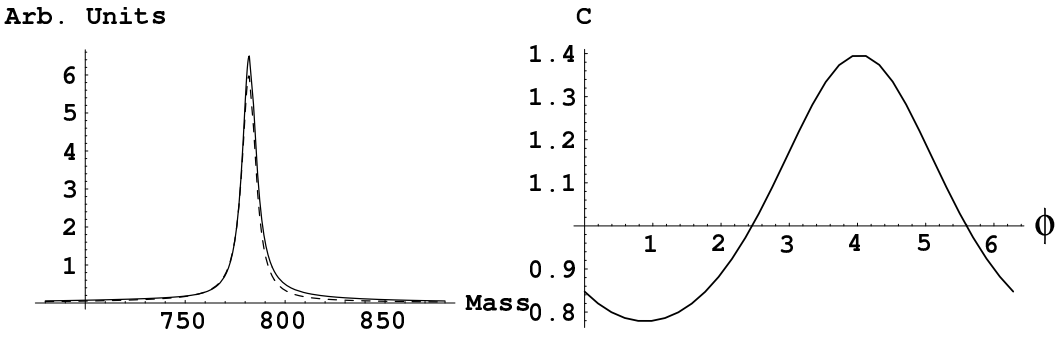

Fig. 16. (a)A plot of coherent equation 10 (solid line) and incoherent equation 11 (dashed line), over the mass range under the ω resonance, with $\phi = -18°$. (b) The correction function, equation 8 plotted as a function of ϕ.